Tuning the Synthesis of Ternary Lead Chalcogenide Quantum Dots by Balancing Precursor Reactivity

Danielle K. Smith,[†,*] Joseph M. Luther,[†] Octavi E. Semonin,[†,‡] Arthur J. Nozik,[†,§] and Matthew C. Beard[†,*]

[†]Center for Advanced Solar Photophysics, Chemical and Materials Sciences, National Renewable Energy Laboratory, Golden, Colorado 80401, United States and [‡]Department of Physics and [§]Department of Chemistry and Biochemistry, University of Colorado, Boulder, Colorado 80309, United States

ABSTRACT We report the synthesis and characterization of composition-tunable ternary lead chalcogenide alloys $PbSe_xTe_{1-x}$, PbS_xTe_{1-x}, and PbS_xSe_{1-x}. This work explores the relative reaction rates of chalcogenide precursors to produce alloyed quantum dots (QDs), and we find the highly reactive bis(trimethylsilyl) (TMS_2)-based precursors allow for the homogeneous incorporation of anions. By varying the Pb to oleic acid ratio, we demonstrate size control of similar composition alloys. We find the resulting QDs are Pb-rich but the Pb/anion ratio is size- and composition-dependent in all alloyed QD as well as in PbSe, PbTe, and PbS QDs and is consistent with the reaction rates of the anion precursors. A more reactive anion precursor results in a lower Pb/anion ratio.

KEYWORDS: alloys · nanoparticles · colloidal quantum dots · heterostructures · lead chalcogenides · ternary

Quantum confinement phenomena are easily explored in the lead chalcogenide family due to the large Bohr radii of bulk excitons (18−200 nm) and ease of synthesis,[1,2] leading to expansive interest for fields such as next generation photovoltaics,[3−5] electronics,[6] optoelectronics,[7] thermoelectrics,[8] and biomedical imaging.[9] Colloidal synthesis lends itself to multistep heterostructured growth,[10−13] but to achieve alloyed structures, a key detail lies in balancing the reactivity of the individual precursors. Alloying is an approach for manipulating optoelectronic properties independent of QD diameter to separate intrinsic and extrinsic factors that influence carrier and excitonic dynamics. For solar energy conversion strategies, alloying can be important for controlling conduction band offsets, localized defect energy levels, and other optoelectronic properties through strain, for example. Recently, electronically coupled PbSe QD films have shown electron and hole mobilities that depend on the QD diameter but not the bandgap.[14] Though debate exists in the literature, a recent publication addressing the controversy shows that multiple exciton generation is more efficient in PbSe QDs compared to bulk PbSe.[15] Alloys can potentially further increase MEG by two possible arguments: (1) disruption of the lattice could provide higher impact-ionization cross sections and (2) tuning of the excited state electronic properties could alter relaxation channels. In many avalanche photodiode materials, it is often alloys that have the most desired attributes.[16,17] Core/shell QDs[10,11] and nanowires[12] of $PbSe/PbS_xSe_{1-x}$ have been reported, and a recent review by Regulacio *et al.*[18] highlights the synthesis of several types of uniform ternary QD alloys including $CdSe_xTe_{1-x}$,[19,20] CdS_xTe_{1-x},[21] CdS_xSe_{1-x},[22] $Bi_{2-x}Sb_xTe_3$,[23] $PbSn_xTe_{1-x}$,[24] and PbS_xSe_{1-x}.[25] Enhanced properties of alloyed nanostructures include adjustable carrier concentrations,[23] improved thermoelectric performance,[23] and higher power conversion efficiency photovoltaics.[25]

Here we explore anion precursors with varying reactivities to produce monodisperse compositionally controlled $PbSe_xTe_{1-x}$, PbS_xTe_{1-x}, and PbS_xSe_{1-x} ternary QD alloys made through a single injection of two seemingly noninteracting anion precursors into a reaction vessel containing a hot Pb-oleate complex. Through careful selection of the precursors, we show that QDs of all ternary alloys within the Pb chalcogenide family can be produced. We speculate that the differing reactivity of the individual precursors may also be responsible for the polydispersity of samples with high Te content and examine the Pb/anion ratio. We measure the extent of anion incorporation with inductively coupled plasma atomic emission spectroscopy (ICP-AES) and X-ray diffraction (XRD) peak positions.

*Address correspondence to danielle.smith@nrel.gov, matt.beard@nrel.gov.

Received for review September 3, 2010 and accepted December 01, 2010.

Published online December 8, 2010. 10.1021/nn102878u

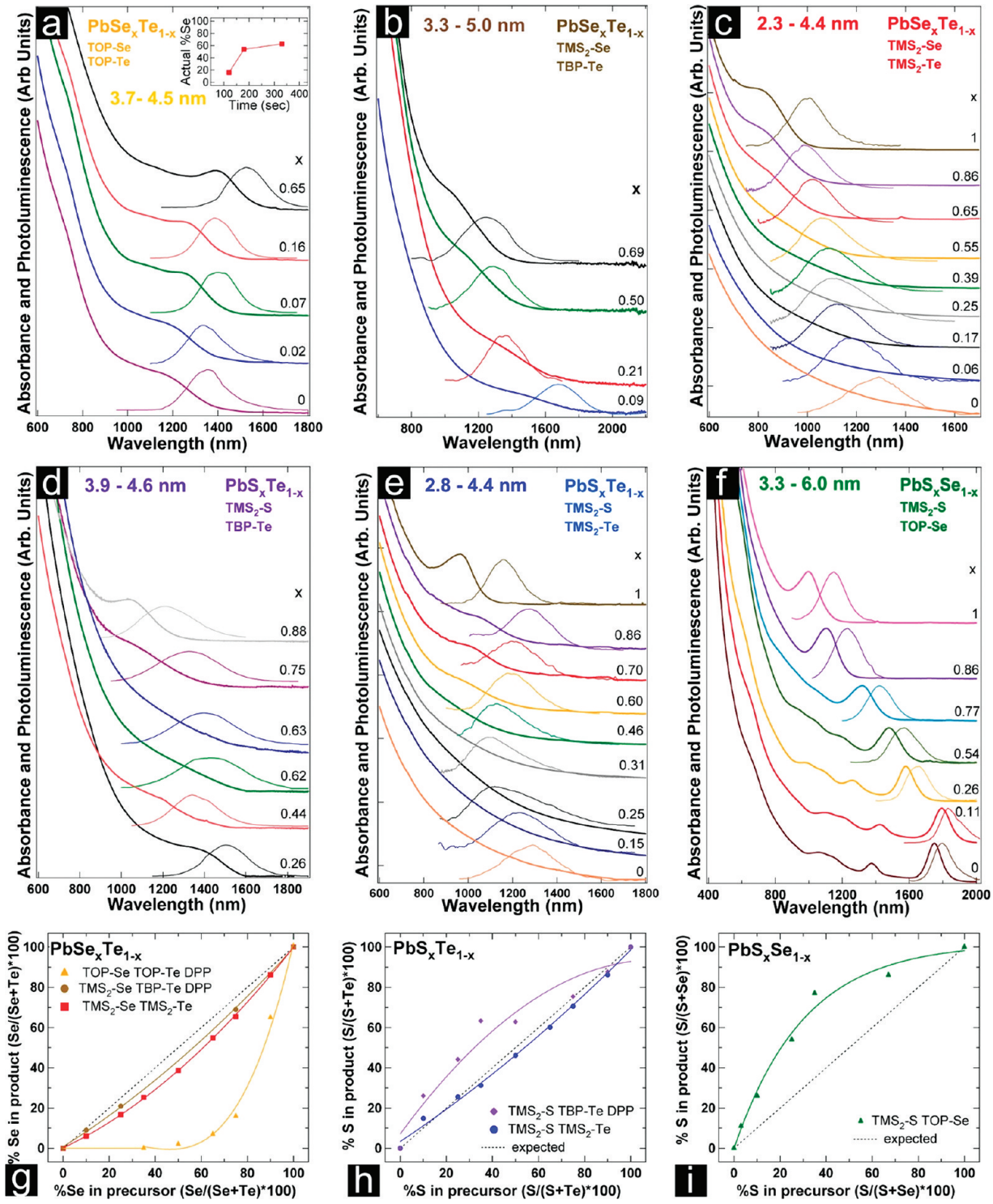

Figure 1. Absorbance and photoluminescence of ternary Pb chalcogenide alloys with varying amounts of each anion: (a) $PbSe_xTe_{1-x}$ QD alloys made from TOP−Se, TOP−Te. (Inset) More Se incorporates with longer reaction times indicating in a gradient structure. (b) $PbSe_xTe_{1-x}$ QD alloys made from TMS_2−Se and TBP−Te, (c) $PbSe_xTe_{1-x}$ made from TMS_2−Se and TMS_2−Te, (d) PbS_xTe_{1-x} QD alloys made from TMS_2−S and TBP−Te, (e) PbS_xTe_{1-x} made from and TMS_2−S and TMS_2−Te, and (f) PbS_xSe_{1-x} made from TMS_2−S and TOP−Se. The QD sizes over the range of compositions were measured with TEM and are reported in each plot. (g−i) ICP-AES data revealing the actual percent of each anion in the alloy QD product versus the percent present in the injection solution. The color of each line in the plots matches the color of the font on the corresponding alloy in parts (a−f). (g)Comparison of the actual amount of Te in $PbSe_xTe_{1-x}$ QD using different Se and Te precursors. (h) Actual percent of Te in PbS_xTe_{1-x} QD product using either TMS_2−Te or TBP−Te as the Te precursor. (i) Actual percent of S in PbS_xSe_{1-x} QD.

RESULTS AND DISCUSSION

Figure 1, panels a−c show the optical properties of $PbSe_xTe_{1-x}$ alloys produced from various precursors, panels d−e are for PbS_xTe_{1-x}, and f is for PbS_xSe_{1-x}. Panels g−i display ICP-AES data comparing the actual anion incorporation versus the injected concentration,

TABLE 1. $PbSe_xTe_{1-x}$ Control Experiments Performed to Verify the Reactivity of Anion Precursors as Suggested by the ICP-AES Data (TMS_2−E > TBP−E > TOP−E)[a]

Se precursor	Te precursor	%Se in product	%Te in product
TBP−Se	TMS_2−Te/ODE	1	99
TBP−Se	TBP−Te	2	98
TBP−Se	TOP−Te	3	97
TMS_2−Se/ODE	TBP−Te	40	60
TBP−Se	TBP−Te	2	98
TOP−Se	TBP−Te	1	99

[a]Experiments were performed using a 50% Se, 50% Te injection solution using either TBP−Se or TBP−Te as a control anion precursor. DPP was not added to these reactions.

which serves as a guide for syntheses. When the reaction rates of both anion precursors are similar, the resulting QD alloy composition matches the anion precursor ratio (indicated by the dashed black line). The QD sizes over the range of compositions were measured from TEM images and are reported in each plot.

Bailey *et al.* reported the synthesis of $CdSe_xTe_{1-x}$ QDs using TOP−Se and TOP−Te[19] and found the reaction kinetics of Te to be twice that of Se. Homogeneous alloys were obtained using a Cd-limited reaction to control the available anion binding sites and maintain a constant Se and Te ratio. When Cd was in excess, a gradient structure consisting of a CdTe core and $CdSe_xTe_{1-x}$ shell was produced. Following Bailey,[19] we attempted the synthesis of homogeneous $PbSe_xTe_{1-x}$ QDs using TOP−Se and TOP−Te using either a 1:1 or 2:1 Pb/(Se+Te) ratio and found the resulting QDs contained much more Te than Se. High Se content alloys are difficult to obtain due to the higher Te reactivity (see Figure 1g, yellow triangles). Contrary to what was reported for the $CdSe_xTe_{1-x}$ system,[19] a higher cation:anion ratio does result in more Se incorporation here. The QDs exhibit higher Se incorporation with longer reaction times (see inset to Figure 1a), suggesting a radial gradient structure supporting the results of Gurusinghe *et al.*[21] and Swafford *et al.*[22] who found that Cd-limited conditions were unable to produce homogeneous CdS_xTe_{1-x} and CdS_xSe_{1-x} alloys.

In the synthesis of CdSe the reaction kinetics of tributylphosphine-selenide (TBP−Se) were found to be 1.7 times faster than TOP−Se,[26] so to increase the incorporation of Se, TBP−Se and bis(trimethylsilyl) selenide (TMS_2−Se) were used. The ICP-AES data and control experiments (see Table 1) show that the reaction rates of the anion precursors are TMS_2−E > TBP−E > TOP−E, where E is used in a general sense to imply chalcogen.

TMS_2−Se in combination with TBP−Te offers higher Se reactivity and allows for alloyed QDs of various compositions to be synthesized (Figures 1b and 1g). In Figure 1g, all of the $PbSe_xTe_{1-x}$ data falls below the dashed line, indicating the reactivity of Te precursors is still greater than Se precursors, but Se and Te incorporation can be better controlled using TMS_2-based precursors for both anions (see Figures 1c and 1g).

For the incorporation of S we employ TMS_2−S to produce both PbS_xTe_{1-x} and PbS_xSe_{1-x}. Figure 1d shows the absorbance spectra of PbS_xTe_{1-x} QDs of varying composition made from TMS_2−S and TBP−Te. Using TBP−Te always resulted in QDs with high S content, as shown in Figure 1h; well controlled PbS_xTe_{1-x} QDs are made from TMS_2−S and TMS_2−Te due to their similar reactivity (see Figure 1e and h).

For PbS_xSe_{1-x}, TMS_2−S and TOP−Se are the precursors, and as reported by Ma,[25] the PbS_xSe_{1-x} QDs always contain more S than expected because TMS_2−S is more reactive than TOP−Se (Figure 1i). Alloy compositions ranging from 0 to 100% S are easily attainable and yield the sharpest exciton transitions, see Figure 1f. The lack of a clear first exciton in alloys with high Te content arises because the 1s and 1p electronic states in PbTe are close in energy and difficult to resolve unless a high monodispersity is achieved.[27] Unfortunately the fast reactivity of TMS_2−Te leads to greater polydispersity (higher σ) in $PbSe_xTe_{1-x}$ and PbS_xTe_{1-x} than PbS_xSe_{1-x} QDs (Figure 2) and increasing polydispersity in PbS_xTe_{1-x} and $PbSe_xTe_{1-x}$ QDs with higher Te content.

Previous literature suggests that DPP reduces lead from Pb^{2+} to Pb^0 increasing the nucleation rate and thus the QD yield,[28,29] however, Evans *et al.* proposed a different scheme where secondary phosphine chalcogenides are the precursors to QD formation because they cause the dissociation a nonreactive Pb-oleate complex and subsequent formation of a reactive Pb-

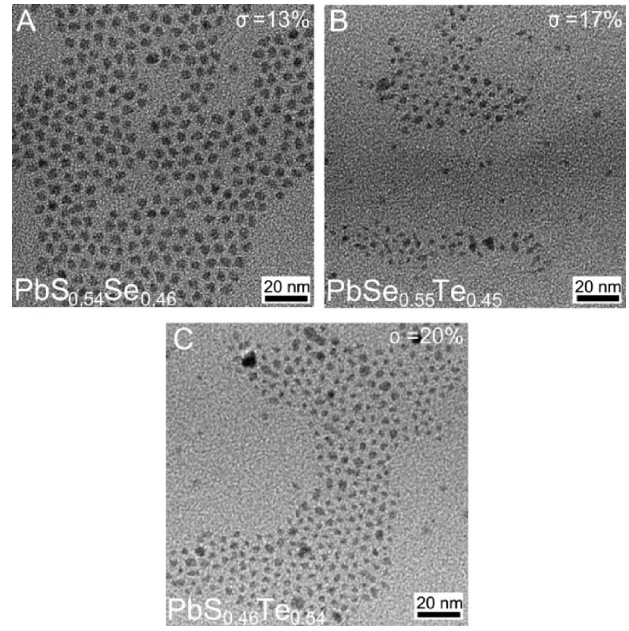

Figure 2. TEM images of (A) $PbS_{0.54}Se_{0.46}$ made from TMS_2−S and TOP−Se (B) $PbSe_{0.55}Te_{0.45}$ made from TMS_2−Se and TMS_2−Te and (C) $PbS_{0.46}Te_{0.54}$ QDs made from TMS_2−S and TMS_2−Te. Due to the fast reactivity of the TMS_2−Te, ternary alloys containing Te are more polydisperse (higher σ) and smaller than PbS_xSe_{1-x}.

TABLE 2. Fitting Coefficients for PbS, PbSe, and PbTe QD Sizing Equations (eq 1)

	bulk E_g	A	B	C
PbS	0.41	0.014494	0.32589	0.07777
PbSe	0.278	0.020866	0.20636	0.42683
PbTe	0.31	0.0026367	0.22721	0.66641

phosphine complex.[30] We find a range of alloy compositions synthesized with either TBP−E or TOP−E cannot easily be achieved in the in the absence of DPP, and $PbSe_xTe_{1-x}$ made from TOP−Se and TOP−Te without DPP contained less than 1% Se (see Table 1). Without the addition of DPP the reactive Pb-phosphine complex does not form and the reaction is dictated by the faster Te precursor reactivity.

The size of the QDs can be tuned by varying the synthetic parameters. Comparing Figures 1a−c reveals that using faster reacting precursors results in QDs of smaller average size. Figure 1f shows that for PbS_xSe_{1-x} QDs, with increasing S the PL blue shifts and the size of the QDs decreases. The same is true for the $PbSe_xTe_{1-x}$ made from TMS_2−Se and TMS_2−Te with increasing Se (Figure 1c). However, for the PbS_xTe_{1-x} made from TMS_2−S and TMS_2−Te, the trend is less clear as the PL does not follow a linear blue shift with the alloy composition (Figure 1e). The QD diameter decreases from 3.2 to 2.6 nm as the amount of S decreases from $PbS_{0.86}Te_{0.14}$ to $PbS_{0.15}Te_{0.85}$. This could be due to optical bowing,[31] which has been observed in $CdSe_xTe_{1-x}$[19] and CdS_xTe_{1-x} alloys.[21] For bulk PbS_xTe_{1-x}, theory predicts either positive[32] or no[33] optical bowing while experimental results on PbS_xTe_{1-x} thin films do not show bowing.[34]

Using established sizing curves for PbS, PbSe, and PbTe, calculations predict how the band gap and QD diameter vary with alloy composition. The size-dependent bandgap of quantum dots can be appropriately fit by the following equation:

$$E_{g,\mathrm{eff}}(d) = E_{g,\mathrm{bulk}} + \frac{1}{Ad^2 + Bd + C} \qquad (1)$$

where $E_{g,\ \mathrm{eff}}$ is the effective bandgap of the quantized crystal in eV, $E_{g,\ \mathrm{bulk}}$ is the bandgap of the semiconductor in bulk form in eV, d is the diameter in nanometers and A, B, and C are fitting coefficients. We use our own sizing of binary QDs for each material and they coincide with various literature values for each.[27,35−37] The fit values appear in Table 2. To construct the composition dependent sizing graphs in Figure 3, a matrix is created from the following alloying equation:

$$E_{g,\mathrm{eff}}(x, d) = x^*E^Y_{g,\mathrm{eff}}(d) + (1 - x)^*E^Z_{g,\mathrm{eff}}(d) \qquad (2)$$

where x is the composition ratio, and Y and Z here refer to the materials in the alloy. Bowing can be considered by simply adding the additional term $-bx(1 - x)$ but the bowing coefficient b has been reported to be very small for Pb chalcogenide alloys (0.03−0.09).[33] We have verified such small bowing by fitting the PbS_xSe_{1-x} size-dependent data in Figure 1f to the full equation to yield a bowing coefficient of 0.09. Figure 3 provides the full range of alloy composition and band gap as a function of size for each of the alloys synthesized in this work. These plots were used to determine the average size of QDs from a known composition and band gap. The difference between these values and those measured with TEM appear in Figure 3 as closed and open circles, respectively. The standard deviation of the average QD size measured by analyzing TEM images is shown in Figure 3 as error bars. There is little difference between the predicted and measured size for the PbS_xSe_{1-x} data as these samples have a clear first exciton in the absorbance due to higher monodispersity and are larger (3.3−6.0 nm) than the $PbSe_xTe_{1-x}$ and PbS_xTe_{1-x} thus making the TEM analysis facile. Greater discrepancy is observed in $PbSe_xTe_{1-x}$ and PbS_xTe_{1-x} with higher Te composition because the first exciton position is difficult to discern and the sample polydispersity and irregular shapes cause inaccurate size estimates. Additionally, the small size (2.3−4.4 nm) of $PbSe_xTe_{1-x}$ and PbS_xTe_{1-x} QDs made from TMS_2−Te and either TMS_2−Se or TMS_2−S are difficult to measure accurately with TEM. The greatest difference between the

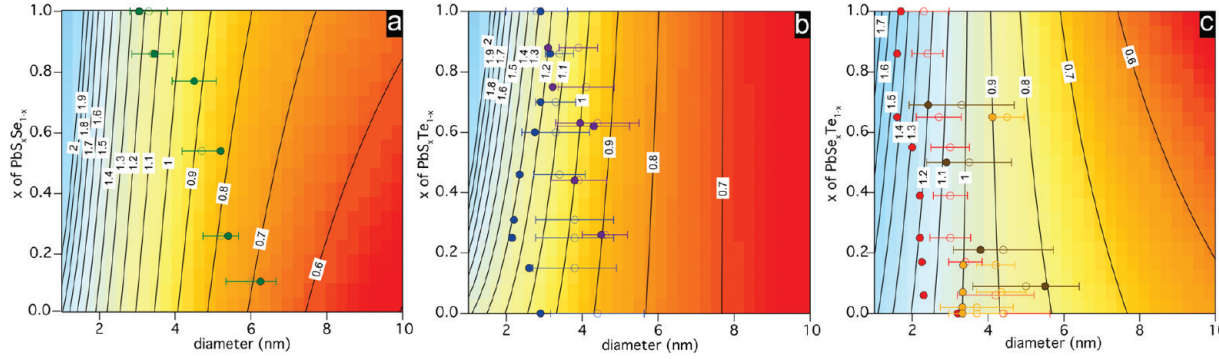

Figure 3. Calculated size- and composition-dependent bandgap of (a) PbS_xSe_{1-x}, (b) PbS_xTe_{1-x}, and (c) $PbSe_xTe_{1-x}$ alloy QDs as described in the text. Bandgap in eV is notated on each contour line. These plots were used to determine the average size of QDs from a known composition and band gap. The difference between these values and those measured with TEM appear as closed and open circles, respectively. Circle colors are: PbS_xSe_{1-x} (green) made from TMS_2−S and TOP−Se, PbS_xTe_{1-x} made from TMS_2−S and TBP−Te (purple), PbS_xTe_{1-x} made from and TMS_2−S and TMS_2−Te (blue), $PbSe_xTe_{1-x}$ made from TOP−Se, TOP−Te (yellow), $PbSe_xTe_{1-x}$ made from TMS_2−Se and TBP−Te (brown), and $PbSe_xTe_{1-x}$ made from TMS_2−Se and TMS_2−Te (red).

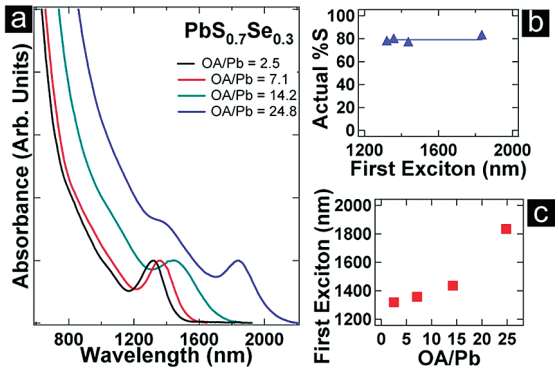

Figure 4. (a) Changing the oleic acid to Pb molar ratio used to synthesize PbS_xSe_{1-x} alloys results in QDs of different size. (b) Actual %S in the PbS_xSe_{1-x} QDs versus first exciton position showing that the S composition is independent of the oleic acid to Pb ratio. (c) PbS_xSe_{1-x} QDs first exciton position versus oleic acid to Pb molar ratio.

predicted and measured values was 1.6 nm and 95% of the predicted sample sizes were within 1 nm of the size determined *via* TEM.

Figure 1 clearly demonstrates that by varying the elemental composition the band gap (or size) of the QDs can be tuned. The QD size can also be varied by altering synthetic conditions including the reaction time and temperature, or Pb to oleic acid molar ratio, as shown in Figure 4. Figure 4a shows the optical properties of $PbS_{0.7}Se_{0.3}$ QDs with an oleic acid to Pb ratio varying from 2.5 to 24.8, the composition remains constant (Figure 4b) while the position of the first exciton varies (Figure 4c) demonstrating the creation of a material with desired size (bandgap) and composition.

Alloy compositions are monitored by X-ray diffraction (XRD) as lattice planes shift based on the average lattice constant created from a uniform mix of anions. All materials studied here exhibit the rock salt structure and have similar lattice constants (5.9362 Å, 6.124 Å, and 6.459 Å for PbS, PbSe, and PbTe respectively). The XRD patterns for $PbSe_xTe_{1-x}$ and PbS_xTe_{1-x} shift from the PbSe/S pattern toward the PbTe pattern as the Te content of the QDs increases (Figure 5). Broader peaks in $PbSe_xTe_{1-x}$ and PbS_xTe_{1-x} samples with high Te content could result from either sample polydispsersity or nonuniform strain in the QDs. If the alloys possess a gradient structure, the lattice constant within the QD would change with the QD radius, giving rise to strain. Because a gradient structure is not observed here (with the exception of the $PbSe_xTe_{1-x}$ made from TOP−Te and TOP−Se as shown in Figure 1a) we believe the peak broadening comes from the sample polydispersity as the samples with high Te content contain many 1−2 nm nanocrystals. For the PbS_xSe_{1-x}, the XRD pattern shifts toward the PbS pattern from the PbSe pattern. All of these trends as well as the (200) peak positions agree with previous reports for ternary alloy lead chalcogenide thin films[34,38,39] and agree with ICP-AES data.

Finally, we compare the ratio of Pb to total anions, rather than the relative ratios of the anions using ICP-AES. Moreels *et al*. proposed that PbSe QDs are faceted spheres with quasi-stoichiometric cores terminated by a Pb surface shell[36] resulting in a size dependent Pb excess. This observation was supported by later work on both PbSe[40] and CdSe.[41] We model Pb/anion ratios for different sizes assuming all surface atoms are Pb, our model is shown in Figure 6 and is calculated as follows:

$$\frac{\mathrm{Pb}}{X} = \frac{D^3 - 4\left(\frac{D}{2} - A\right)^3}{4\left(\frac{D}{2} - A\right)^3} \qquad (3)$$

where D is the QD diameter in nanometers and A is the covalent radius of Pb = 0.146 nm.[42] The radius is used instead of the diameter because the model as-

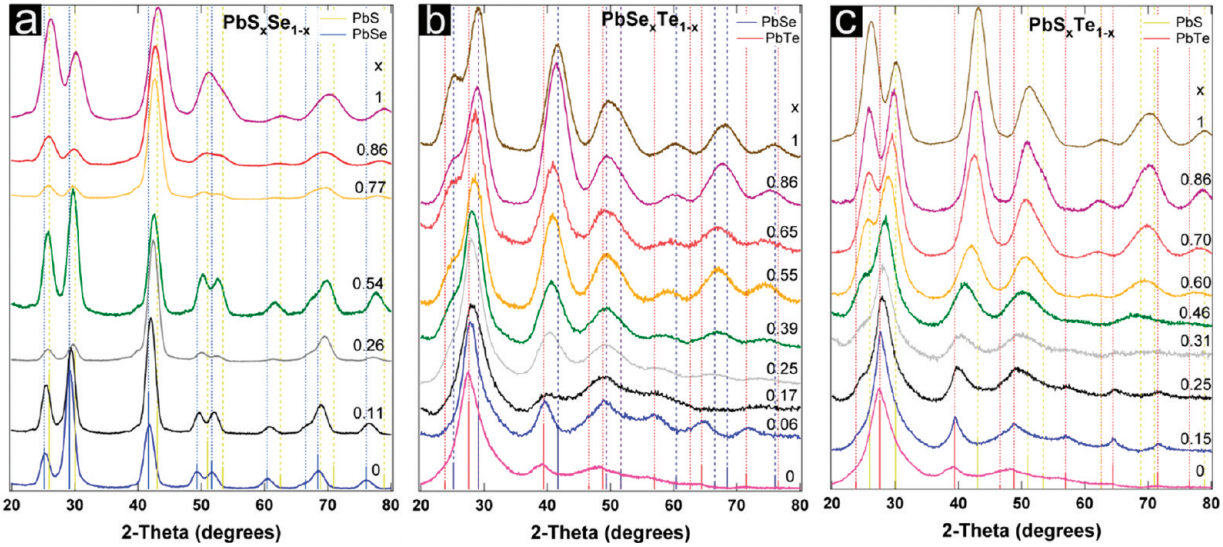

Figure 5. XRD patterns of different (a) PbS_xSe_{1-x} made from TMS_2−S and TOP−Se (b) $PbSe_xTe_{1-x}$ made from TMS_2−Se and TMS_2−Te, and (c) PbS_xTe_{1-x} made from and TMS_2−S and TMS_2−Te. The red, blue, and yellow vertical lines are the patterns of PbTe, PbSe, and PbS, respectively. A large (220) peak relative to the other diffraction peaks for PbS_xSe_{1-x} indicates texturing of QDs with [200] direction perpendicular to the XRD substrate.

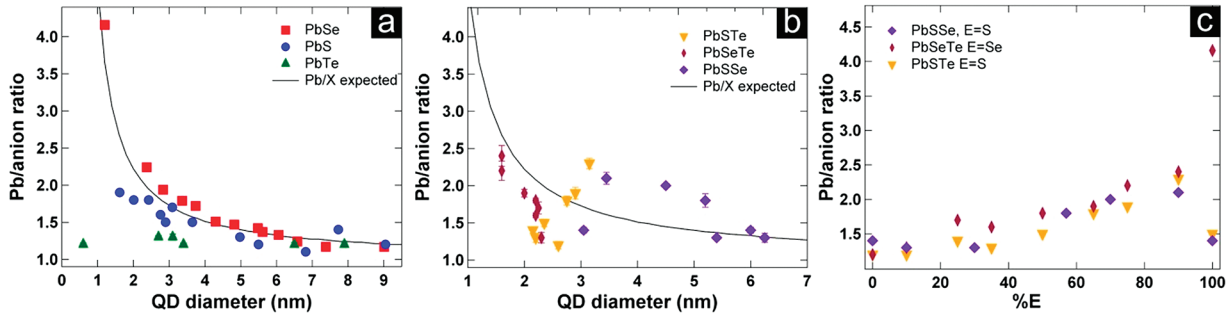

Figure 6. Cation (Pb) to anion ratios for (a) PbSe, PbS, PbTe, and (b) $PbSe_xTe_{1-x}$, PbS_xSe_{1-x}, and PbS_xTe_{1-x} QDs. QD sizes were determined with the sizing curves appearing in Figure 3. The black line is a model predicting Pb/anion ratios if all exposed atoms on the surface are Pb. (c) Pb/anion ratio of the alloys as a function of anion composition.

sumes an average half monolayer of excess Pb, as excess Pb atoms add only to exposed Se atoms.[36] As the QD diameter is reduced, the percentage of atoms on the surface increases resulting in higher Pb/anion ratios. We measured Pb/E for PbSe, PbS, and PbTe QDs, and find that the model accounts for the data for all PbSe QDs, but for PbS QDs there is a deviation when the diameter is less than 2 nm. For PbTe, the ratio is found to be 1.2−1.3 and size independent. We speculate that these trends are related to the reaction rates of the different anion precursors; faster reaction rates result in less excess Pb in the reaction solution and lower Pb/anion ratios. The smallest PbTe sample (0.6 nm) was made using TMS_2−Te, PbS is always synthesized using TMS_2−S, and the smallest PbSe (1.1 nm) used TMS_2−Se. Based on the ICP-AES data, the reaction rates of the TMS_2−E precursors can be deduced as follows: TMS_2−Te ≥ TMS_2−S > TMS_2−Se (which differs from the trend observed for phosphine chalcogenides: Te > Se > S).[26] Thus the Pb/anion ratio for the small QDs follows the trend PbTe ≤ PbS < PbSe. For QDs greater than 2 nm, PbSe was made with TOP−Se and PbTe was produced with TOP−Te and the Pb/anion ratios are PbTe < PbSe as the reactivity of TOP−Te > TOP−Se. However, PbS QDs larger than 2 nm were made with TMS_2−S (more reactive than TOP−Te) so the higher Pb/anion ratios for PbS than PbTe are unexpected.

For the $PbSe_xTe_{1-x}$ QDs, the Pb/(Se+Te) ratio falls from 2.5 to 1.3 (Figure 6b and c) as the amount of Se decreases from 90% to 10%. In the PbS_xTe_{1-x} QDs, the Pb/(S+Te) ratio falls from 2.3 to 1.2 as the amount of S decreases from 90% to 10% while the PbS_xSe_{1-x} QD Pb/(S + Se) ratio falls from 2.1 to 1.3 as the amount of S decreases from 90 to 10%. These trends are consistent with the observed values for PbTe (a Pb/Te ratio of 1.2−1.3 that is size independent), PbSe (Pb/Se = 2.2−1.2 with decreasing size) and PbS (Pb/S = 1.7−1.1 with decreasing size) QDs of corresponding size. The presence of lower Pb/anion ratios with increased amounts of Te also is expected as Pb/Te ratios are size independent.

CONCLUSIONS

This work explores the relative reaction rates of chalcogenide precursors to produce alloyed QDs of $PbSe_xTe_{1-x}$, PbS_xSe_{1-x}, and PbS_xTe_{1-x}. The sharpest exciton transitions were observed in PbS_xSe_{1-x}, and using highly reactive TMS_2-based precursors allowed for incorporation of anions in each family. Furthermore, size control of similar composition alloys was obtained by varying the ligand concentration. Exploring the Pb/anion ratio revealed a size and composition dependent Pb excess in all alloyed QD as well as in PbSe, PbTe, and PbS and is consistent with the reaction rates of the anion precursors.

METHODS

Materials and Supplies. All chemicals are used as received. Lead oxide (PbO, 99.995%) is purchased from Alfa Aesar. Oleic acid (OA, 90%), 1-octadecene (ODE, 90%), bis(trimethylsilyl) sulfide (TMS_2−Se), selenium powder (99.99%), trioctylphosphine (TOP, 90%), tributylphosphine (TBP, ≥93.5%), diphenylphosphine (DPP, 98%), anhydrous ethanol (≥99.5%), anhydrous hexane (95%), and anhydrous tetrachloroethylene (TCE, ≥99.9%) are purchased from Sigma-Aldrich. Bis(trimethylsilyl) telluride (TMS_2−Te) and bis(trimethylsilyl) selenide (TMS_2−Se) are pur-

TABLE 3. List of Which Anion Precursor Is Used for Making Each Ternary Pb Chalcogenide Alloy QD Sample

sample	S precursor	Se precursor	Te precursor	DPP
$PbSe_xTe_{1-x}$ made from TOP−Se and TOP−Te	n/a	1 M TOP−Se	0.75 M TOP−Te	15 μL
$PbSe_xTe_{1-x}$ made from TBP−Se and TOP−Te	n/a	0.75 M TBP−Se	0.75 M TOP−Te	15 μL
$PbSe_xTe_{1-x}$ made from TMS_2−Se and TBP−Te	n/a	0.5 M TMS_2−Se/ODE	0.75 M TBP−Te	15 μL
$PbSe_xTe_{1-x}$ made from TMS_2−Se and TMS_2−Te	n/a	0.5 M TMS_2−Se/ODE	0.5 M TMS_2−Te/ODE	n/a
PbS_xTe_{1-x} QDs made from TMS_2−S and TBP−Te	0.75 M TMS_2−S/ODE	n/a	0.75 M TBP−Te	15 μL
PbS_xTe_{1-x} QDs made from TMS_2−S and TMS_2−Te	0.75 M TMS_2−S/ODE	n/a	0.5 M TMS_2−Te/ODE	n/a
PbS_xSe_{1-x}[25]	TMS_2−S	1 M TOP−Se	n/a	37 μL

chased from Gelest. Nitric acid (HNO_3) is purchased from Fisher. Doubly distilled deionized water (DI-H_2O) is used for ICP-AES sample preparation.

Quantum Dot Synthesis. All of the alloyed QDs are synthesized using a one-pot, hot injection method on a Schlenk line using standard air-free techniques. For all reactions except where noted 0.223 g PbO, 0.7 g OA, and 5 g ODE are degassed and dried at 140 °C for at least 1 h in a 50 mL round-bottom flask under N_2. Approximately 3 mL of 0.5 mM chalcogen prepared anion solution is then injected. The reaction proceeds for 40 s and is quenched by immersing the flask in a water bath. Once the temperature decreases to 70 °C, 5 mL of anhydrous hexane is injected and the reaction flask is allowed to cool to ambient temperature. All anion solutions are prepared in a glovebox with excess ODE to bring the solution volume to 3 mL. The solutions are prepared by mixing the desired amount of each anion precursor as shown in Table 3.

After cooling to room temperature, the reaction solution is transferred into centrifuge tubes under air-free conditions and then spun for 3 min at 6000 rpm to eliminate any solid byproducts, poorly capped QDs, or aggregates that precipitate. Anhydrous hexane and anhydrous ethanol are used as a solvent/nonsolvent pair to precipitate the QDs in a centrifuge operated for 5 min at 6000 rpm. Two washing steps are used and the QDs are stored as a dried powder for later use.

Sample Characterization. XRD is performed on a Scintag X1 diffractometer using Bragg−Brentano geometry and Cu Kα radiation (λ = 1.54 Å). Samples are prepared by dropcasting concentrated solutions onto quartz substrates. XRD patterns are compared to that of PbS (JCPDS #05−0592), PbSe (JCPDS #06−0354) and PbTe (JCPDS #38−1435).

TEM pictures are obtained using a FEI Tecnai G2 20 Twin microscope with a LaB_6 filament operated at 200 kV. Images are digitally acquired with a 4 mega-pixel Gatan UltraScan 1000 camera. TEM samples are prepared by dropcasting QDs dispersed in hexane onto carbon coated copper 200 mesh TEM grids (Electron Microscopy Sciences).

The optical properties of the QDs are obtained using UV−visible near-infrared absorbance and photoluminescence (PL) spectroscopy. All spectroscopic measurements are performed on as-prepared samples without postsynthesis size selection. Measurements are taken at room temperature with the QDs dispersed in TCE in quartz cuvettes with a 1 cm path length. Absorbance spectra are acquired using a Shimadzu UV-3600 spectrophotometer. PL spectra are acquired using a PTI Quantamaster QM 4/2003 steady-state spectrofluorometer. A steady-state 150 W xenon arc lamp chopped at 22 Hz serving as the excitation source, and an InGaAs diode detector is used to record the PL.

ICP-AES is performed on a Varian Liberty 150 spectrometer with Plasma 96 software by Micron Software, Inc., to determine the relative Pb, Te, Se and S amount in each QD sample. Pb is measured at 283.306 eV, S at 180.731 eV, Se at 196.026 eV, and Te at 214.281 eV. A calibration solution containing 100 ppm each of Pb, S, Se, and Te in 5% HNO_3 is purchased from Inorganic Ventures. The samples are prepared by adding 1 mL of HNO_3 to 2 mg of dried QDs in a 20 mL vial. The samples are allowed to fully digest before 19 mL of DI-H_2O water is added, producing a final concentration of ~100 ppm in 5% HNO_3. ICP-AES operating conditions are 1500 650 V PMT voltage, 15 L/min plasma gas flow, 1.5 L/min auxiliary gas flow, and peristaltic pump speed 15 rpm. The sample uptake time is 30 s.

Acknowledgment. Financial support is provided by the Center for Advanced Solar Photophysics, an Energy Frontier Research Center funded by US Department of Energy, Office of Science, Office of Basic Energy Sciences. DOE funding was provided to NREL through contract DE-AC36-08G028308. We acknowledge the Biomass Surface Characterization Laboratory at NREL for use of their TEM.

REFERENCES AND NOTES

1. Rogach, A. L.; Eychmuller, A.; Hickey, S. G.; Kershaw, S. V. Infrared-Emitting Colloidal Nanocrystals: Synthesis, Assembly, Spectroscopy, and Applications. *Small* **2007**, *3*, 536–557.
2. Wise, F. W. Lead Salt Quantum Dots: The Limit of Strong Quantum Confinement. *Acc. Chem. Res.* **2000**, *33*, 773–780.
3. Johnston, K. W.; Pattantyus-Abraham, A. G.; Clifford, J. P.; Myrskog, S. H.; MacNeil, D. D.; Levina, L.; Sargent, E. H. Schottky-Quantum Dot Photovoltaics for Efficient Infrared Power Conversion. *Appl. Phys. Lett.* **2008**, *92*, 3.
4. Luther, J. M.; Gao, J.; Lloyd, M. T.; Semonin, O. E.; Beard, M. C.; Nozik, A. J. Stability Assessment on a 3% Bilayer PbS/ZnO Quantum Dot Heterojunction Solar Cell. *Adv. Mater.* **2010**, *22*, 3704–3707.
5. Luther, J. M.; Law, M.; Beard, M. C.; Song, Q.; Reese, M. O.; Ellingson, R. J.; Nozik, A. J. Schottky Solar Cells Based on Colloidal Nanocrystal Films. *Nano Lett.* **2008**, *8*, 3488–3492.
6. Talapin, D. V.; Murray, C. B. PbSe Nanocrystal Solids for n- and p-Channel Thin Film Field-Effect Transistors. *Science* **2005**, *310*, 86–89.
7. Konstantatos, G.; Howard, I.; Fischer, A.; Hoogland, S.; Clifford, J.; Klem, E.; Levina, L.; Sargent, E. H. Ultrasensitive Solution-Cast Quantum Dot Photodetectors. *Nature* **2006**, *442*, 180–183.
8. Dresselhaus, M.; Chen, G.; Tang, M.; Yang, R.; Lee, H.; Wang, D.; Ren, Z.; Fleurial, J. P.; Gogna, P. New Directions for Low-Dimensional Thermoelectric Materials. *Adv. Mater.* **2007**, *19*, 1043–1053.
9. Etgar, L.; Lifshitz, E.; Tannenbaum, R. Hierarchical Conjugate Structure of Gamma-Fe_2O_3 Nanoparticles and PbSe Quantum Dots for Biological Applications. *J. Phys. Chem. C* **2007**, *111*, 6238–6244.
10. Brumer, M.; Kigel, A.; Amirav, L.; Sashchiuk, A.; Solomesch, O.; Tessler, N.; Lifshitz, E. PbSe/PbS and PbSe/$PbSe_xS_{1-x}$ Core/Shell Nanoparticles. *Adv. Funct. Mater.* **2005**, *15*, 1111–1116.
11. Lifshitz, E.; Brumer, M.; Kigel, A.; Sashchiuk, A.; Bashouti, M.; Sirota, M.; Galun, E.; Burshtein, Z.; Le Quang, A. Q.; Ledoux-Rak, I.; et al. Stable PbSe/PbS and PbSe/$PbSe_xS_{1-x}$ Core-Shell Nanocrystal Quantum Dots and Their Applications. *J. Phys. Chem. B* **2006**, *110*, 25356–25365.
12. Mokari, T.; Habas, S. E.; Zhang, M. J.; Yang, P. D. Synthesis of Lead Chalcogenide Alloy and Core-Shell Nanowires. *Angew. Chem., Int. Ed.* **2008**, *47*, 5605–5608.
13. Sashchiuk, A.; Langof, L.; Chaim, R.; Lifshitz, E. Synthesis and Characterization of PbSe and PbSe/PbS Core-Shell Colloidal Nanocrystals. *J. Cryst. Growth* **2002**, *240*, 431–438.
14. Liu, Y.; Gibbs, M.; Puthussery, J.; Gaik, S.; Ihly, R.; Hillhouse, H. W.; Law, M. Dependence of Carrier Mobility on Nanocrystal Size and Ligand Length in PbSe Nanocrystal Solids. *Nano Lett.* **2010**, *10*, 1960–1969.
15. Beard, M. C.; Midgett, A. G.; Hanna, M. C.; Luther, J. M.; Hughes, B. K.; Nozik, A. J. Comparing Multiple Exciton Generation in Quantum Dots To Impact Ionization in Bulk Semiconductors: Implications for Enhancement of Solar Energy Conversion. *Nano Lett.* **2010**, *10*, 3019–3027.
16. David, J. P. R.; Tan, C. H. Material Considerations for Avalanche Photodiodes. *IEEE J. Sel. Top. Quantum Electron.* **2008**, *14*, 998–1009.
17. Makarovsky, O.; Feu, W. H. M.; Patane, A.; Eaves, L.; Zhuang, Q. D.; Krier, A.; Beanland, R.; Airey, R. Hot Electron Transport and Impact Ionization in the Narrow Energy Gap $InAs_{1-x}N_x$ Alloy. *Appl. Phys. Lett.* **2010**, *96*, 3.
18. Regulacio, M. D.; Han, M. Y. Composition-Tunable Alloyed Semiconductor Nanocrystals. *Acc. Chem. Res.* **2010**, *43*, 621–630.
19. Bailey, R. E.; Nie, S. M. Alloyed Semiconductor Quantum Dots: Tuning the Optical Properties without Changing the Particle Size. *J. Am. Chem. Soc.* **2003**, *125*, 7100–7106.
20. Wang, R.; Calvignanello, O.; Ratcliffe, C. I.; Wu, X.; Leek, D. M.; Zaman, M. B.; Kingston, D.; Ripmeester, J. A.; Yu, K. Homogeneously-Alloyed CdTeSe Single-Sized Nanocrystals with Bandgap Photoluminescence. *J. Phys. Chem. C* **2009**, *113*, 3402–3408.
21. Gurusinghe, N. P.; Hewa-Kasakarage, N. N.; Zamkov, M. Composition-Tunable Properties of CdS_xTe_{1-x} Alloy Nanocrystals. *J. Phys. Chem. C* **2008**, *112*, 12795–12800.
22. Swafford, L. A.; Weigand, L. A.; Bowers, M. J.; McBride, J. R.; Rapaport, J. L.; Watt, T. L.; Dixit, S. K.; Feldman, L. C.; Rosenthal, S. J. Homogeneously Alloyed CdS_xSe_{1-x} Nanocrystals: Synthesis, Characterization, and

Composition/Size-Dependent band gap. *J. Am. Chem. Soc.* **2006**, *128*, 12299–12306.
23. Zhao, Y. X.; Dyck, J. S.; Hernandez, B. M.; Burda, C. Enhancing Thermoelectric Performance of Ternary Nanocrystals through Adjusting Carrier Concentration. *J. Am. Chem. Soc.* **2010**, *132*, 4982–4983.
24. Arachchige, I. U.; Kanatzidis, M. G. Anomalous Band Gap Evolution from Band Inversion in $Pb_{1-x}Sn_xTe$ Nanocrystals. *Nano Lett.* **2009**, *9*, 1583–1587.
25. Ma, W.; Luther, J. M.; Zheng, H. M.; Wu, Y.; Alivisatos, A. P. Photovoltaic Devices Employing Ternary PbS_xSe_{1-x} Nanocrystals. *Nano Lett.* **2009**, *9*, 1699–1703.
26. Liu, H.; Owen, J. S.; Alivisatos, A. P. Mechanistic Study of Precursor Evolution in Colloidal Group II-VI Semiconductor Nanocrystal Synthesis. *J. Am. Chem. Soc.* **2006**, *129*, 305–312.
27. Murphy, J. E.; Beard, M. C.; Norman, A. G.; Ahrenkiel, S. P.; Johnson, J. C.; Yu, P. R.; Micic, O. I.; Ellingson, R. J.; Nozik, A. J. PbTe Colloidal Nanocrystals: Synthesis, Characterization, and Multiple Exciton Generation. *J. Am. Chem. Soc.* **2006**, *128*, 3241–3247.
28. Steckel, J. S.; Yen, B. K. H.; Oertel, D. C.; Bawendi, M. G. On the Mechanism of Lead Chalcogenide Nanocrystal Formation. *J. Am. Chem. Soc.* **2006**, *128*, 13032–13033.
29. Joo, J.; Pietryga, J. M.; McGuire, J. A.; Jeon, S. H.; Williams, D. J.; Wang, H. L.; Klimov, V. I. A Reduction Pathway in the Synthesis of PbSe Nanocrystal Quantum Dots. *J. Am. Chem. Soc.* **2009**, *131*, 10620–10628.
30. Evans, C. M.; Evans, M. E.; Krauss, T. D. Mysteries of TOPSe Revealed: Insights into Quantum Dot Nucleation. *J. Am. Chem. Soc.* **2010**, *132*, 10973–10975.
31. Bernard, J. E.; Zunger, A. Electronic-Structure of ZnS, ZnSe, ZnTe, and Their Pseudobinary Alloys. *Phys. Rev. B* **1987**, *36*, 3199–3228.
32. Zaoui, A.; Kacimi, S.; Zaoui, M.; Bouhafs, B. Theoretical Investigation of Electronic Structure of PbS_xTe_{1-x} and $PbSe_xTe_{1-x}$ Alloys. *Mater. Chem. Phys.* **2009**, *114*, 650–655.
33. Wei, S.-H.; Zunger, A. Electronic and Structural Anomalies in Lead Chalcogenides. *Phys. Rev. B: Condens. Matter* **1997**, *55*, 13605–10.
34. Kumar, S.; Khan, M. A. M.; Zulfequar, M.; Husain, M. Optical, Structural and Electrical Investigations on $PbTe_{1-x}S_x$ Alloys. *J. Mater. Sci.* **2007**, *42*, 363–367.
35. Cademartiri, L.; Montanari, E.; Calestani, G.; Migliori, A.; Guagliardi, A.; Ozin, G. A. Size-Dependent Extinction Coefficients of PbS Quantum Dots. *J. Am. Chem. Soc.* **2006**, *128*, 10337–10346.
36. Moreels, I.; Lambert, K.; De Muynck, D.; Vanhaecke, F.; Poelman, D.; Martins, J. C.; Allan, G.; Hens, Z. Composition and Size-Dependent Extinction Coefficient of Colloidal PbSe Quantum Dots. *Chem. Mater.* **2007**, *19*, 6101–6106.
37. Moreels, I.; Lambert, K.; Smeets, D.; De Muynck, D.; Nollet, T.; Martins, J. C.; Vanhaecke, F.; Vantomme, A.; Delerue, C.; Allan, G.; et al. Size-Dependent Optical Properties of Colloidal PbS Quantum Dots. *ACS Nano* **2009**, *3*, 3023–3030.
38. Kumar, S.; Hussain, M.; Sharma, T. P.; Husain, M. Characterization of $PbSe_{1-x}Te_x$ Thin Films. *J. Phys. Chem. Solids* **2003**, *64*, 367–376.
39. Kumar, S.; Khan, M. A. M.; Khan, S. A.; Husain, M. Studies on Vacuum Evaporated $PbS_{1-x}Se_x$ Thin Films. *Opt. Mater.* **2004**, *25*, 25–32.
40. Dai, Q. Q.; Wang, Y. N.; Li, X. B.; Zhang, Y.; Pellegrino, D. J.; Zhao, M. X.; Zou, B.; Seo, J.; Wang, Y. D.; Yu, W. W. Size-Dependent Composition and Molar Extinction Coefficient of PbSe Semiconductor Nanocrystals. *ACS Nano* **2009**, *3*, 1518–1524.
41. Morris-Cohen, A. J.; Frederick, M. T.; Lilly, G. D.; McArthur, E. A.; Weiss, E. A. Organic Surfactant-Controlled Composition of the Surfaces of CdSe Quantum Dots. *J. Phys. Chem. Lett.* **2010**, 1078–1081.
42. Cordero, B.; Gomez, V.; Platero-Prats, A. E.; Reves, M.; Echeverria, J.; Cremades, E.; Barragan, F.; Alvarez, S. Covalent Radii Revisited. *Dalton Trans.* **2008**, 2832–2838.